Published in final edited form as:
Biochim Biophys Acta. 2013 December ; 1833(12): . doi:10.1016/j.bbamcr.2013.09.015.

Regulation of Autophagic Flux by Dynein-mediated Autophagosomes Trafficking in Mouse Coronary Arterial Myocytes

Ming Xu[1], **Xiao-Xue Li**[1], **Jing Xiong**[1], **Min Xia**[1], **Erich Gulbins**[2], **Yang Zhang**[1], and **Pin-Lan Li**[1]

[1]Department of Pharmacology and Toxicology, School of Medicine, Virginia Commonwealth University, Richmond, VA, 23298

[2]Department of Molecular Biology, University of Duisburg-Essen, Hufelandstrasse 55, 45122, Essen, Germany

Abstract

Autophagic flux is an important process during autophagy maturation in coronary arterial myocytes (CAMs). Here, we defined the role and molecular mechanism of the motor protein dynein in the regulation of autophagic flux in CAMs. In mouse CAMs, dynein protein is abundantly expressed. Pharmacological or genetic inhibition of dynein activity dramatically enhanced 7-ketocholesterol (7-Ket)-induced expression of the autophagic marker LC3B and increased the cellular levels of p62, a selective substrate for autophagy. Inhibition of dynein activity increased 7-Ket-induced formation of autophagosomes (APs), but reduced the number of autophagolysosomes (APLs) in CAMs. Furthermore, 7-Ket increased the fusion of APs with lysosomes and the velocity of APs movement in mouse CAMs, which was abolished when the dynein activity in these cells was inhibited. Interestingly, 7-Ket increased lysosomal Ca^{2+} release and stimulated dynein ATPase activity, both of which were abolished by NAADP antagonists, NED-19 and PPADS. Taken together, our data suggest that NAADP-mediated Ca^{2+} release plays a crucial role in regulating dynein activity, which mediates APs trafficking and fusion with lysosomes to form APLs thus regulating autophagic flux in CAMs under atherogenic stimulation.

Keywords

Dynein; Autophagy; 7-ketocholesterol; NAADP; Lysosome

Introduction

Autophagy (also known as macroautophagy) is a cellular catabolic pathway leading to lysosomal degradation and recycling of proteins and organelles in eukaryotes [1]. A growing body of evidence suggests that autophagy is stimulated in advanced atherosclerotic plaques by oxidized lipids, inflammation, and metabolic stress [2]. It is suggested that autophagy

Correspondence sent to: Pin-Lan Li, MD, PhD, Department of Pharmacology and Toxicology, Medical College of Virginia, Virginia Commonwealth University, 1220 East Broad Street, P.O. Box 980613, Richmond, VA 23298 ; Tel. 804 828-4793 ; Fax: 804 828-2117 ; pli@vcu.edu.

may have both protective and detrimental roles during atherosclerosis, depending upon the status of autophagy or stages of atherosclerosis [2–4]. Although the molecular mechanisms for autophagy have been extensively studied since the discovery of mammalian autophagy genes (Atg genes), it remains largely unknown how autophagy is regulated in smooth muscle cells (SMCs) in the pathogenesis of coronary atherosclerosis. 7-Ketocholesterol (7-Ket) is a major oxidation product of cholesterol found at high levels in atherosclerotic plaques and is even more atherogenic than cholesterol in some animal studies [5–6]. 7-Ket regulates the expression of autophagic genes [7]. Therefore, 7-Ket was chosen as atherogenic stimulus in the present study to detect the regulatory mechanisms of autophagy in mouse coronary arterial myocytes (CAMs).

Upon induction of autophagy, nascent double-membraned autophagic vacuoles (autophagosomes, APs) are formed to sequester a cargo, such as protein aggregates, damaged organelles, or pathogens [8]. Late stage APs fuse with lysosomes to form autophagolysosomes (APLs), where the cargo is degraded by lysosomal hydrolases [9]. This APL formation together with the lysosomal degradation process is also known as autophagic flux. In mammalian cells, there are multiple sites of autophagosomes (APs) formation, thus the APs need to be trafficked and transported to the lysosomes implicating that a specific transport system may be present. The molecular details of this transport process are unknown. Here we investigated a potential role of dynein ATPase in this process. Dynein ATPase is a multi-subunit cytoplasmic motor protein, which is responsible for nearly all minus-end microtubule-based transport of vesicles within mammalian cells [10]. Dynein regulates a variety of intracellular motile processes including mitosis, maintenance of the Golgi apparatus and trafficking of membranous vesicles and other intracellular particles [11]. Recent studies have demonstrated that dynein is involved in AP trafficking to meet with lysosomes to form APLs [12–16]. Inhibition or loss of dynein function has been demonstrated to cause impaired AP fusion with lysosomes or increased number of APs in glioma or neuronal cells [17]. Based on these observations, we hypothesized that dynein contributes to the fusion of APs with lysosome to form APLs and consequent autophagy flux in CAMs under proatherogenic stimulation.

Here, we demonstrate that the atherogenic stimulus 7-Ket enhances autophagy in CAMs and triggers a dynein-mediated APs trafficking and fusion with lysosomes. Lysosome-dependent NAADP-sensitive Ca^{2+} release participates in the regulation of dynein ATPase activity.

Materials and methods

Mice

Mice were purchased from the Jackson Laboratory. Eight-week old male and female mice were used in all experiments. All experimental protocols were reviewed and approved by the Institutional Animal Care and Use Committee of Virginia Commonwealth University.

Isolation and culture of mouse CAMs

CAMs were isolated from mice as previously described [18]. In brief, mice were deeply anesthetized with an intraperitoneal injection of pentobarbital sodium (25 mg/kg). The heart was excised with an intact aortic arch and immersed in a petri dish filled with ice-cold Krebs-Henseleit (*KH*) solution (in mM: 20 HEPES, 128 NaCl, 2.5 KCl, 2.7 $CaCl_2$, 1 $MgCl_2$, 16 glucose, pH 7.4). A 25-gauge needle filled with Hank's buffered saline solution (HBSS) (in mM: 5.0 KCl, 0.3 KH_2PO_4, 138 NaCl, 4.0 $NaHCO_3$, 0.3 $Na_2HPO_4{\cdot}7H_2O$, 5.6 D-glucose, and 10.0 HEPES, with 2% antibiotics) was inserted into the aortic lumen while the whole heart remained in the ice-cold buffer solution. The tip of the needle was inserted deep into the heart close to the aortic valve. The needle was tied in place with the needle tip as

close to the base of the heart as possible. The infusion pump was started with a 20-ml syringe containing warm HBSS through an intravenous extension set at a rate of 0.1 ml/min for 15 min. HBSS was replaced with a warm enzyme solution (1 mg/ml collagenase type I, 0.5 mg/ml soybean trypsin inhibitor, 3% BSA, and 2% antibiotic-antimycotic), which was flushed through the heart at a rate of 0.1 ml/min. Perfusion fluid was collected at 30-, 60-, and 90-min intervals. At 90 min, the heart was cut with scissors and the apex was opened to flush out the cells that collected inside the ventricle. The fluid was centrifuged at 1, 000 rpm for 10 min, the cell-rich pellets were mixed with the one of the media described below, and the cells were plated on 2% gelatin-coated six-well plates and incubated in 5% CO_2-95% O_2 at 37°C. DMEM supplemented with 10% FBS, 10% mouse serum, and 2% antibiotics was used to culture isolated smooth muscle cells. The medium was replaced three days after cell isolation and then once or twice each week until the cells grew to confluence. As previously described [19], mouse CAMs were identified according to their morphology, immunohistological staining, Western blot analysis of marker proteins, and flow cytometric characteristics.

Demonstration of dynein expression in coronary arterial myocytes

For reverse transcriptase PCR (RT-PCR) analysis, total RNA was isolated from primary cultured CAMs by Trizole (Invitrogen, CA, USA), and 50, 100 and 200 ng of different amount of total RNA was transcribed to cDNA according to the instructions of the first strand cDNA synthesis kit manufacturer (Bio-Rad, Hercules, CA, USA). These synthesized cDNAs were used for dynein PCR reaction by PCR Supermix (Invitrogen) with primers of 5′-GCCAGTTACAGGAACCTCACG-3′ and 5′-CCAGAAGGATGTACCAGCCATT-3′ at a final concentration of 200 nM. β-actin was used as control with primers of 5′-TCGCTGCGCTGGTCGTC -3′ and 5′-GGCCTCGTCACCCACATAGGA-3′. A negative control was performed to verify the PCR condition, which contained all the components of the PCR except the template DNA. The PCR products were separated by 1.2% agarose gel for confirmation of product size.

Cell homogenates of 10, 20, and 40 μg from primary cultures of CAMs were used for Western blot analysis as described previously [20]. An anti-dynein antibody from Santa Cruz (SC-80295, 1:200) was used to probe dynein protein and β-actin was used as loading control.

Transfection of dynamitin cDNA

Transfection of dynamitin cDNA (MC200162, OriGene Technologies) was performed using the TransFectin Lipid Reagent (Bio-Rad, CA, USA) according to the manufacturer's instructions, as we described previously [20]. The efficiency of dynamitin cDNA transfection was assessed by Western blot analyses. Dynamitin antibody was purchased from Santa Cruz Biotechnology (SC-135135; 1:200).

Flow cytometric detection of APs and APLs

The Cyto-ID Autophagy Detection Kit (Enzo Life Sciences, Cat. No. ENZ-51031-K200) was used to detect APs. Briefly, CAMs (1×10^5/ml) were collected and centrifuged (400 × *g*, 5 minutes) at the end of the treatment. Then, CAMs were incubated with 0.5 mL of freshly diluted Cyto-ID Green Detection Reagent (1:4000) for 30 minutes at 37°C in the dark. Without washing, stained CAMs were run in the green (FL1) channel with a Guava Easycyte Mini Flow Cytometry System (Guava Technologies, Hayward, CA) and analyzed with Guava acquisition and analysis software (Guava Technologies). The enhancement of Cyto-ID Green dye signal indicates an increase in APs.

In addition, acridine orange (Sigma) was used to detect APLs. CAMs (1×10^6/ml) were stained with acridine orange (1:5000) for 17 min. After washes, CAMs were harvested in phenol red-free growth medium. Green (510–530 nm) and red (>650 nm) fluorescence emission from 10^4 cells illuminated with blue (488 nm) excitation light was measured with Flow Cytometry System and analyzed with Guava acquisition and analysis software. The ratio of mean red/green fluorescence intensity from live cells gated by FSC/SSC was calculated to indicate the change of intracellular APLs.

Confocal microscopic analysis of co-localization of lysosomes with APs in CAMs

BacMam (baculovirus-based expression in mammalian cells) expression system was utilized to deliver and express LC3B-GFP and Lamp1-RFP genes in CAMs. Modified insect virus (baculovirus) expressing a fusion construct of LC3B-GFP (P36235, Invitrogen) or Lamp1-RFP (C10597, Invitrogen) were packaged as BacMam virus particles. CAMs (4×10^4/ml) cultured in 35 mm dish were incubated with 12 μl mixture of BacMam virus particles containing LC3B-GFP or Lamp1-RFP gene at 37°C for 24 hours. Then, the cells were replaced with fresh medium and ready for treatment. The fluorescent images for APs (LC3B-GFP) and lysosomes (Lamp1-RFP) in CAMs were recorded at an excitation/emission (nm) of 485/520 and 555/584. Then the colocalizations were visualized with confocal microscopy. The colocalization coefficiency of LC3B-GFP and Lysosomes-RFP was analyzed with Image-Pro Plus 6.0 software as we previously described [21].

Dynamic analysis of AP movement in CAMs

CAMs (2×10^4/ml) cultured in 35 mm dish were incubated with 12 μl BacMam GFP-LC3B virus particles at 37°C for 16 h to express the LC3B-GFP gene. The confocal fluorescent microscopic recording was conducted with an Olympus Fluoview System. The fluorescent images for APs (LC3B-GFP) of the CAMs were continuously recorded at an excitation/emission (nm) of 485/520 by using XYT recording mode with a speed of 1 frame/10 second for 10 min. Vesicle tracking was performed in MAGEJ using the LSM reader and Manual tracking plugins according to the published protocol [12]. Ten vesicles with GFP-LC3B were chosen at random for each cell. These vesicles were then tracked manually for as long as they were visible, while the program calculated velocities for each frame. All the results were further calculated and analyzed in Excel. The number of cells with different velocity of APs was calculated.

Fluorescent microscopic measurement of $[Ca^{2+}]_i$ in CAMs

A fluorescence image analysis system was used to determine $[Ca^{2+}]_i$ in CAMs with fura-2 acetoxymethyl ester (fura-2) as an indicator as previously described [19, 22], Having been loaded with 10 μM fura-2 at room temperature for 30 min, the cells were washed three times with Ca^{2+}-free Hank's buffer. The ratio of fura-2 emissions, when excited at the wavelengths of 340 and 380 nm, was recorded with a digital camera (Nikon Diaphoto TMD Inverted Microscope). Metafluor imaging and analysis software were used to acquire, digitize, and store the images for off-line processing and statistical analysis (Universal Imaging). The fluorescence ratio of excitation at 340 nm to that at 380 nm (F340/F380) was determined after background subtraction, and $[Ca^{2+}]_i$ was calculated by using the following equation: $[Ca^{2+}]_i = K_d\beta[(R - R_{min})/(R_{max} - R)]$, where K_d for the fura-2-Ca^{2+} complex is 224 nM; R is the fluorescence ratio (F_{340}/F_{380}); R_{max} and R_{min} are the maximal and minimal fluorescence ratios measured by addition of 10 μM of Ca^{2+} ionophore ionomycin to Ca^{2+}-replete solution (2.5 mM $CaCl_2$) and Ca^{2+}-free solution (5 mM EGTA), respectively; and β is the fluorescence ratio at 380-nm excitation determined at R_{min} and R_{max}, respectively. Lysosomal Ca^{2+} release was monitored indirectly by treating Fura-2-loaded

CAMs with Glycyl-L-phenylalanine 2-naphthylamide (GPN, 200 μM), a tripeptide causing osmotic lysis of cathepsin C–positive lysosomes.

Fluorescent confocal microscopic measurement of lysosome Ca^{2+} release

To detect lysosome Ca^{2+} release, sub-confluent CAMs in 35-mm cell culture dishes were incubated with dextran-conjugated tetramethylrhodamine (Rho; 1 mg/ml; Molecular Probes) for 4 h in DMEM medium containing 10% FBS at 37°C, 5% CO_2, followed by a 20-h chase in dye-free medium for lysosomes loaded with Rho as previously described [23–24]. After being washed with Hank's buffered saline solution (HBSS) (in mM: 5.0 KCl, 0.3 KH_2PO_4, 138 NaCl, 4.0 $NaHCO_3$, 0.3 $Na_2HPO_4{\cdot}7H_2O$, 5.6 D-glucose, and 10.0 HEPES, with 2% antibiotics) three times, the Rho-loaded cells were then incubated with the Ca^{2+}-sensitive dye fluo-4 at a concentration of 5 μM. Ca^{2+} release and lysosome trace recordings were performed. Lysosome/Rho (Lyso/Rho) fluorescence images were acquired at 568-nm excitation and 590-nm emission. The co-localization coefficiency of Ca^{2+}/fluo-4 and Lyso/Rho was analyzed with Image-Pro Plus 6.0 software [25].

Assay of cytoplasmic dynein ATPase activity

Dynein in mouse CAMs was purified using a published protocol with slight modification [26]. Cytoplasmic protein of mouse CAMs was extracted with ice-cold extraction buffer (250 ml of 0.05 M PIPES-NaOH, 0.05 M HEPES, pH 7.0, containing 2 mM $MgC1_2$, 1 mM EDTA, 1 mM phenylmethylsulfonyl fluoride (PMSF), 10 μg/ml leupeptin, 10μg/ml tosyl arginine methyl ester (TAME), 1 μg/ml pepstatin A, and 1 mM dithiothreitol (DTT). Exogenous taxol (20 μM) was added to 20 mL of cell extract containing 4 mg/mL cytoplasmic protein, which was incubated in a 37°C water bath (with occasional swirling) for 12 min. The cell extract was underlayered with a prewarmed 7.5% sucrose solution, and then centrifuged at 60,000 *g* for 30 min at 35°C. The supernatant was removed and the pellet was resuspended in 10 mL of extraction buffer containing 3 mM MgGTP and 5 μM taxol to release kinesin and dynamin. The resuspended pellet was incubated for 15 min prior to centrifugation at 60,000 *g* for 30 min. The supernatant was removed, and the pellet was resuspended in 1.25 mL of extraction buffer containing 10 mM Mg-ATP for 10 min at 37°C. The resuspended pellet was centrifuged at 200,000 *g* for 30 min at 25°C. The supernatant containing ATP-released cytoplasmic dynein was used for sucrose density gradient fractionation. Cytoplasmic dynein may constitute up to 50% of total protein in the ATP extract, the remainder consisting of tubulin and a low level of fibrous microtubule-associated proteins (MAPs). 1 mL ATP extract was further centrifuged on 10 mL of a 5–20% sucrose gradient in fractionation buffer (20 mM Tris-HCl, pH 7.6, 50 mM KCl, 5 mM $MgSO_4$, 0.5 mM EDTA and 1 mM DTT) at 125,000 *g* for 16 h at 4°C. Eleven 1 mL fractions were collected from the bottom of the tube. The dynein fraction peak at about fraction 5, well resolved from the other tubulin and MAPs.

The assays of dynein ATPase activity were performed in 50 μL reaction mixtures containing 20 mM Tris-HCl (pH 7.6), 50 mM KCl, 5 mM $MgSO_4$, 0.5 mM EDTA and 1 mM DTT [27]. In a standard assay condition, 10 μL of enzyme fractions and 4 mM of ATP were incubated with assay buffer at 37 °C for 40 min. The reaction was then stopped using highly acidic malachite green reagent and the absorbance was read at 660 nm in spectrophotometer (Elx800, Bio-Tek). The amount of inorganic phosphate release in the enzymatic reaction was calculated using the standard calibration curve generated with inorganic phosphate. The control in this assay contained all ingredients of the reaction mixture but the reaction was stopped at 0 time.

Statistics

Data are presented as means ± SE. Significant differences between and within multiple groups were examined using ANOVA for repeated measures, followed by Duncan's multiple-range test. The Students *t* test was used to detect significant differences between two groups. $P<0.05$ was considered statistically significant.

Results

Inhibition of dynein increased the protein expression of LC3B and p62

To demonstrate the presence of dynein in the CAMs, we first measured the expression of mRNA and protein of dynein by RT-PCR and Western blot analysis. Supplemental Fig. 1A showed a typical gel document of RT-PCR products of dynein and β-actin, respectively. The normalized intensity ratio of dynein to β-actin is summarized in supplemental Fig. 1B. No significant difference among the different total RNA groups was found, which indicated that the amount of dynein RT-PCR production was proportional to total RNA quantity. Most importantly, Western blot studies (Supplemental Fig 1C) and the summarized intensity ratio of dynein to β-actin (Supplemental Fig. 1D) show expression of dynein in CAMs. The intensity of individual dynein bands is proportional to the amounts of CAMs homogenates loaded. These results demonstrate expression of dynein in mouse CAMs.

The mammalian target of rapamycin (mTOR) is a serine/threonine kinase that plays an integral role in the regulation of many cellular processes, including transcription, translation, cell size, cytoskeletal organization and autophagy. The immunosuppressive drug rapamycin induces autophagysome formation in a wide variety of cell types and species by inhibiting the activity of mTOR complex 1 (mTORC1) [28–29]. In addition, rapamycin also regulates autophagosome fusion with lysosome and autophagic flux [12, 30]. Therefore, rapamycin was used as a positive control in the present study. Microtubule-associated protein 1 light chain 3 beta (LC3B) is an autophagy marker protein, which is recruited to autophagosomal membranes during the formation of APs. p62 is a selective substrate of the autophagy degrading pathway. Protein expression of LC3B significantly increased in CAMs that were exposed to 7-Ket or rapamycin (Fig. 1A and 1B). Inhibition of dynein ATPase by EHNA (erythro-9-[3–(2-Hydroxynonyl) adenine) further increased LC3B expression in CAMs under control conditions or with 7-Ket or rapamycin. These results suggest that more APs were formed or accumulated in CAMs treated with EHNA. Similarly, the abundance of p62 was higher in CAMs pretreated with EHNA (Fig. 1C and 1D), suggesting that less p62 protein was degraded possibly due to impaired autophagic flux by EHNA.

Next, we further investigated the role of dynein for protein expression of LC3B and p62 in CAMs with dynamitin overexpression, which was shown to disrupt and inhibit the dynein complex. To this end, we transfected dynamitin cDNA into CAMs resulting in a 5-fold overexpression of dynamitin (supplemental Fig. 2A and 2B). We then analyzed expression of LC3B and p62. Similar to EHNA, transfection of dynamitin enhanced the expression of LC3B and p62 in CAMs under control condition or with 7-Ket or rapamycin treatment (Fig. 2A–2D).

Dynein is involved in the formation of APLs and APs

We also used flow cytometry to analyze the formation of APLs in CAMs with a lysomotrophic dye, acridine orange, which accumulates in lysosomes with bright red fluorescence and shows bright green and dim red fluorescence in the cytoplasm and nucleolus. Since APLs accumulate more acridine orange than lysosomes, the red/green fluorescence ratio indirectly indicates the change of intracellular APLs [31]. Fig. 3A shows that CAMs treated by 7-Ket or rapamycin shifted up to the area with high red fluorescence

intensity, which was inhibited in CAMs with EHNA. Quantification of the data in Fig. 3B and 3C indicated that 7-Ket or rapamycin significantly increased the red/green fluorescence ratio suggesting that APLs were formed. However, such 7-Ket or rapamycin-induced APL formation was markedly attenuated in CAMs with dynein inhibitor EHNA or dynamitin overexpression.

Next, we examined whether reduced APL formation leads to accumulation of APs in CAMs. Recently, a flow cytometry analysis using Cyto-ID Green dye has been demonstrated to be a rapid and quantitative approach to monitor autophagy in live cells [32]. The Cyto-ID Green dye selectively labels autophagic vacuoles including pre-autophagosomes, APs and APLs. Thus, an impaired autophagic flux will result in increased number of autophagic vacuoles and enhanced Cyto-ID Green fluorescence. Fig.4A and 4B showed that 7-Ket or rapamycin increased the percentage of Cyto-ID-positive cells from 6.0% to 10.6% or 16.7%, respectively. Such 7-Ket or rapamycin-induced increases was further augmented in CAMs with dynein inhibitor EHNA or dynamitin overexpression.

Inhibition of dynein activity prevents lysosome fusion

Lamp1, a lysosomal marker protein belonging to a type 1 integral membrane protein, is highly expressed in lysosomal membranes [33]. To directly investigate the fusion of APs with lysosomes in living cells, we introduced LC3B-GFP and Lamp1-RFP genes into CAMs by BacMam expression system to express both proteins that were located to APs and lysosomes, respectively. As shown in Fig. 5A, yellow punctuates or patches in the overlaid images labeled as area of interest (AOI) represented the colocalization of LC3B and Lamp1. Under control conditions, only a few yellow dots were detected. The co-localization of LC3B and Lamp-1 was increased by upon 7-Ket or rapamycin treatment, indicating a higher interaction or fusion of lysosomes with APs (Fig. 5A–C). This colocalization was significantly attenuated by EHNA or transfection of dynamitin cDNA (Fig. 5A–C).

Dynamic analysis to APs movement

APs are formed randomly throughout the cytoplasm. However, the majority of lysosomes are localized in the perinuclear region. Thus, APs need to be transported in the cytoplasm to fuse with lysosome. To test a role of dynein in APs movement to lysosomes, we labeled APs in living CAMs with LC3B-GFP by BacMam technique. Typically, fluorescent images of CAMs were taken every 10 seconds (Fig. 6A). Under control condition, APs moved bidirectionally, i.e. towards and away from the nucleus. When CAMs were treated with 7-Ket, the movement of APs was enhanced (Fig. 6A). The velocity of AP movement significantly increased from 0.01 mm/second to 0.09 mm/second (Fig. 6B and 6C). EHNA-treatment or transfection of dynamitin cDNA almost completely abolished all movement of APs in the velocity-range between 0.04 mm/second and 0.09 mm/second. Similar results were also found in the CAMs treated with rapamycin with or without EHNA or dynamitin cDNA (not shown).

NAADP mediated 7-Ket-induced lysosomal Ca^{2+} release

To test whether lysosomal Ca^{2+} was involved in APs trafficking, fluorescent imaging analysis was conducted to test the lysosomal Ca^{2+} release in intact CAMs. GPN was used to release Ca^{2+} from lysosomes by inducing their selective osmotic swelling. 7-Ket doubled GPN-induced Ca^{2+} release, which was blocked by NAADP antagonists, NED-19 or PPADS (Fig. 7A and 7B). To confirm this data we employed an independent method to detect lysosomal Ca^{2+} release, i.e. we measured the localization of Ca^{2+} around lysosomes by confocal microscopy after labeling cells with fluo-4. Ca^{2+} release regions co-localized with lysosomes as indicated by yellow spots formed by green fluo-4 signals with rhodamine-red lysosomal marker (Lyso/Rho) (Fig. 8A). Quantification of the data revealed a significant

increase in the colocalization coefficiency of fluo-4-Ca^{2+} and Lyso/Rho in CAMs when they were treated with 7-Ket or rapamycin. Lysosomal Ca^{2+} release by 7-Ket or rapamycin was abolished by pretreatment of CAMs with PPADS or NED-19.

NAADP-dependent lysosome Ca^{2+} controls dynein ATPase activity

Our data indicates that dynein controls AP movement in CAMs upon treatment with 7-Ket or rapamycin. Thus, we tested whether 7-Ket or rapamycin also regulate the activity of dynein ATPase. Treatment of CAMs with 7-Ket resulted in a much higher dynein ATPase activity than control CAMs (Fig. 9), which was significantly attenuated by EHNA, PPADS or NED-19.

Discussion

In the present study, we demonstrated that upon atherogenic stimulus, autophagy, in particular, autophagic flux, is significantly enhanced in CAMs. Microtubule motor protein dynein mediates APs trafficking and fusion with lysosomes, which consequently contributes to autophagic flux. Lysosome-dependent NAADP-sensitive Ca^{2+} release participates in the regulation of dynein ATPase activity.

Accumulating evidence indicates that the role of autophagy in the vascular SMCs can be both protective and detrimental during the development of atherosclerosis [34]. For example, at the early stage of atherosclerosis, moderately enhanced autophagy safeguards plaque cells against oxidative stress by degrading the damaged material or engulf defective mitochondria to limit the release of proapoptotic proteins such as cytochrome c [3, 35]. In addition, increased autophagy in CAMs may stabilize CAMs in the contractile phenotype to prevent these cells from proliferation and growth [36–37]. However, excessive autophagy in SMCs may result in autophagic cell death leading to plaque destabilization, thereby evoking atherothrombosis, myocardial infarction or stroke [2, 35, 38–40]. Thus, the roles of autophagy in atherosclerosis depend upon the status of autophagy and vascular cell types. The present study attempted to explore the detailed molecular mechanisms that regulate autophagy in the pathogenesis of atherosclerosis. During autophagy, APs are generated *de novo* to sequester cytoplasmic proteins and organelles, which are delivered to lysosomes for degradation. After formation, APs show a rapid vectorial movement in the direction of the centrosome, where lysosomes are usually concentrated [12]. It was previously reported that APs move in a microtubule- and dynein-dynactin motor complex-dependent manner [41]. Here, we demonstrated that dynein has a similar function in cells exposed to proatherogenic stimuli.

LC3B is mammalian orthologue of Atg8 in yeast, which specifically associates with AP membranes [42]. Upon fusion with the lysosome, LC3B is degraded on the inner phagolysosomal membrane [14]. The present study demonstrated that 7-Ket induced expression of LC3B protein, indicating an increase in the number of APs in CAMs exposed to proatherogenic stimuli. It further confirms that proatherogenic stimulation can activate autophagy pathway, which is consistent with previous reports [7]. Importantly, the protein levels of LC3B was further enhanced in CAMs by inhibition of dynein both under resting conditions and after proatherogenic stimulation, suggesting that more autophagic vacuoles were formed or accumulated in CAMs lacking dynein ATPase activity. In addition, p62 protein also accumulated in cells after inhibition of dynein upon proatherogenic stimulation by 7-Ket. Since p62, also called sequestosome 1(SQSTM1), binds directly to LC3B and thereby triggers autophagic degradation of p62-positive cytoplasmic inclusion bodies [43], the accumulation of p62 protein suggests a failed breakdown of APs and demonstrates that autophagic flux was impaired in CAMs after inhibition of dynein. These results support the view that dynein plays a key role in autophagy under atherogenic stimulus, presumably

because less APs can be targeted by lysosomes for the breakdown process in CAMs lacking dynein activity, consequently increasing the number of APs. This function is also consistent with our observation that inhibition of dynein in CAMs reduced the formation of APLs. In addition, we confirmed a reduced autophagic flux in CAMs with dynein inhibition using Cyto-ID Green detection reagent, which is a novel dye that selectively labels autophagic vacuoles in live cells and monitors autophagic flux. This novel method confirms the notion that 7-Ket enhances AP formation in CAMs, which further increased upon inhibition of dynein activity, while the formation of APLs is reduced upon dynein inhibition. This notion is also confirmed by our data using LC3B-GFP and Lamp1-RFP. Two different types of fusion can be observed between APs and lysosome. First, a complete fusion of APs with lysosomes results in a completely double-labeled hybrid vesicle. Second, a more often observed fusion belongs to the 'kiss-and-run' type [31]. When they eventually separate, the lysosome retains the transferred content from APs. Thus, both kind of fusion is likely to result in the colocalizaion of LC3B-GFP with Lamp1-RFP, which was significantly induced by 7-Ket in the present study. Inhibition of dynein ATPase activity prevented this fusion event under proatherogenic stimuli.

Our data on the movement of APs within a cell provide insight into the mechanisms how dynein controls lysosome-AP fusion and the formation of APLs. We found that the movement of APs was activated in 7-Ket treated cells, which was prevented by inhibition of dynein. This data strongly supports the view that dynein controls trafficking and fusion of APs to lysosomes in CAMs. Recent studies have demonstrated that defective autophagic flux may influence cell signaling pathways such as Wnt activity leading to fibrosis [44] or collagen degradation in cardiomyoctes [44]. In this regard, our study may provide a mechanistic link between impaired dynein function and atherogenesis. Under proatherogenic stimulation, enhanced autophagic flux may down-regulate signaling pathways controlling cell dedifferentiation, proliferation and growth, or levels of extracellular matrix proteins via autophagolysosomal degradation machinery. The loss of dynein function in CAMs impairs AP-lysosome fusion, resulting in decreased formation of APLs and impaired breakdown of autophagic contents. Such defective autophagic flux may activate cell dedifferentiation, proliferation and growth, and/or accumulation of extracellular matrix proteins, all of which ultimately contribute to coronary arterial smooth muscle remodeling and ultimately induce or accelerate atherosclerosis.

7-Ket is found abundant in oxidized low density lipoprotein (ox-LDL), which has been demonstrated to enhance the expression of beclin-1 and LC3B in vascular smooth muscle cells [45]. Thus, in the present study, we used 7-Ket as a prototype atherogenic stimulus to study the role of dynein in regulating autophagy. Given the fact that many other atherogenic stimulation including inflammation, ER stress, hypoxia and metabolic stress induce autophagy [1–2], the present study implicates that similar role of dynein may be present in CAMs under these non-lipid athergenic stimulations. In addition to smooth muscle cells, atherogenic stimulation by ox-LDL induced autophagy in endothelial cells, which protect cells from apoptosis and thus endothelial cell damage [46–47] or lead to degradation of ox-LDL [48]. Therefore, it is possible that loss of dynein activity may reduce autophagy or autophagolysosomal degradation of ox-LDL in these endothelial cells leading to endothelial dysfunction.

Finally, we analyzed what mechanisms controlled dynein activity under proatherogenic stimuli. Dynein is subject to a wide array of regulatory inputs [49]. Direct binding of Ca^{2+} to a component of the dynein complex has been reported to regulate dynein motor function and the distribution of cytoplasmic dynein [50–51]. Lysosomes contain high levels of Ca^{2+}, which serves as an important intracellular Ca^{2+} store as does the sarcoplasmic reticulum [52]. Lysosomal Ca^{2+} can be mobilized or released to mediate molecular trafficking or

recycling and to control vesicular fusion events associated with lysosomes [53–54]. NAADP, a CD38-ADP-ribosylcyclase product, is one of the most potent intracellular Ca^{2+} mobilizing molecules, which may regulate lysosomal Ca^{2+} release and lysosome function through its action on the transient receptor potential (TRP)-ML1 (mucolipin-1) channels [55–56], or through other mechanisms such as two-pore channels [57]. NAADP has been recognized as a fundamental signaling mechanism regulating a variety of cell or organ functions in different biological systems[57]. In the present study, we demonstrated that proatherogenic stimulation enhanced lysosomal Ca^{2+} release, which was markedly reduced by NAADP antagonists in CAMs. This data suggests that NAADP-dependent lysosomal Ca^{2+} release was involved in 7-Ket stimulation in CAMs, which is consistent with a report that 7-Ket can trigger a sustained increase of cytosolic-free Ca^{2+} [58]. To further clarify if NAADP-dependent lysosomal Ca^{2+} regulates dynein activity during 7-Ket stimulation, we tested the activity of dynein ATPase in CAMs. Dynein contains two identical heavy chains, which contain the ATPase activity and are thus responsible for generating movement that move cargo along the microtubule. In the present study, we found that 7-Ket dramatically enhanced the dynein ATPase activity, which was almost completely inhibited by NAADP inhibitors. This data suggests that 7-Ket induces NAADP production resulting in release of lysosomal Ca^{2+} and activation of dynein ATPase activity in CAMs. Moreover, we found that NAADP antagonists can mimic the effect of EHNA on APs and APLs (supplemental Figure 3). To our knowledge, these results for the first time provide evidence that a NAADP-dependent lysosomal Ca^{2+} burst regulates dynein activity and consequent autophagy under proatherogenic stimuli in CAMs.

In conclusion, we demonstrated that under atherogenic stimulus, autophagy was significantly enhanced in CAMs via lysosome-dependent NAADP-sensitive Ca^{2+} release. In this model, NAADP-sensitive Ca^{2+} release regulates dynein activity that critically controls the trafficking of APs and lysosomes to encounter each other leading to APL formation and autophagic flux in CAMs.

Supplementary Material

Refer to Web version on PubMed Central for supplementary material.

Acknowledgments

The study was supported by grants from the National Institute of Health (HL057244, HL075316, and HL091464).

References

1. Levine B, Kroemer G. Autophagy in the pathogenesis of disease. Cell. 2008; 132:27–42. [PubMed: 18191218]
2. Martinet W, De Meyer GR. Autophagy in atherosclerosis. Curr Atheroscler Rep. 2008; 10:216–223. [PubMed: 18489849]
3. Martinet W, De Meyer GR. Autophagy in atherosclerosis: a cell survival and death phenomenon with therapeutic potential. Circ Res. 2009; 104:304–317. [PubMed: 19213965]
4. Fuster JJ, Fernandez P, Gonzalez-Navarro H, Silvestre C, Nabah YN, Andres V. Control of cell proliferation in atherosclerosis: insights from animal models and human studies. Cardiovasc Res. 2010; 86:254–264. [PubMed: 19900964]
5. Lyons MA, Brown AJ. 7-Ketocholesterol. Int J Biochem Cell Biol. 1999; 31:369–375. [PubMed: 10224662]
6. Stadler N, Lindner RA, Davies MJ. Direct detection and quantification of transition metal ions in human atherosclerotic plaques: evidence for the presence of elevated levels of iron and copper. Arterioscler Thromb Vasc Biol. 2004; 24:949–954. [PubMed: 15001454]

7. Martinet W, Schrijvers DM, Timmermans JP, Bult H. Interactions between cell death induced by statins and 7-ketocholesterol in rabbit aorta smooth muscle cells. Br J Pharmacol. 2008; 154:1236–1246. [PubMed: 18469840]
8. Martinet W, Knaapen MW, Kockx MM, De Meyer GR. Autophagy in cardiovascular disease. Trends Mol Med. 2007; 13:482–491. [PubMed: 18029229]
9. Ryter SW, Lee SJ, Smith A, Choi AM. Autophagy in vascular disease. Proc Am Thorac Soc. 2010; 7:40–47. [PubMed: 20160147]
10. Oiwa K, Sakakibara H. Recent progress in dynein structure and mechanism. Curr Opin Cell Biol. 2005; 17:98–103. [PubMed: 15661525]
11. Vallee R. Molecular analysis of the microtubule motor dynein. Proc Natl Acad Sci U S A. 1993; 90:8769–8772. [PubMed: 8415604]
12. Jahreiss L, Menzies FM, Rubinsztein DC. The itinerary of autophagosomes: from peripheral formation to kiss-and-run fusion with lysosomes. Traffic. 2008; 9:574–587. [PubMed: 18182013]
13. Kochl R, Hu XW, Chan EY, Tooze SA. Microtubules facilitate autophagosome formation and fusion of autophagosomes with endosomes. Traffic. 2006; 7:129–145. [PubMed: 16420522]
14. Xie Z, Klionsky DJ. Autophagosome formation: core machinery and adaptations. Nat Cell Biol. 2007; 9:1102–1109. [PubMed: 17909521]
15. Yamamoto M, Suzuki SO, Himeno M. The effects of dynein inhibition on the autophagic pathway in glioma cells. Neuropathology. 2010; 30:1–6. [PubMed: 19496938]
16. Rubinsztein DC, Ravikumar B, Acevedo-Arozena A, Imarisio S, O'Kane CJ, Brown SD. Dyneins, autophagy, aggregation and neurodegeneration. Autophagy. 2005; 1:177–178. [PubMed: 16874055]
17. Ravikumar B, Acevedo-Arozena A, Imarisio S, Berger Z, Vacher C, O'Kane CJ, Brown SD, Rubinsztein DC. Dynein mutations impair autophagic clearance of aggregate-prone proteins. Nat Genet. 2005; 37:771–776. [PubMed: 15980862]
18. Teng B, Ansari HR, Oldenburg PJ, Schnermann J, Mustafa SJ. Isolation and characterization of coronary endothelial and smooth muscle cells from A1 adenosine receptor-knockout mice. Am J Physiol Heart Circ Physiol. 2006; 290:H1713–H1720. [PubMed: 16299260]
19. Xu M, Zhang Y, Xia M, Li XX, Ritter JK, Zhang F, Li PL. NAD(P)H oxidase-dependent intracellular and extracellular O2*- production in coronary arterial myocytes from CD38 knockout mice. Free Radic Biol Med. 2012; 52:357–365. [PubMed: 22100343]
20. Xu M, Xia M, Li XX, Han WQ, Boini KM, Zhang F, Zhang Y, Ritter JK, Li PL. Requirement of translocated lysosomal V1 H(+)-ATPase for activation of membrane acid sphingomyelinase and raft clustering in coronary endothelial cells. Mol Biol Cell. 2012; 23:1546–1557. [PubMed: 22357614]
21. Xia M, Zhang C, Boini KM, Thacker AM, Li PL. Membrane raft-lysosome redox signalling platforms in coronary endothelial dysfunction induced by adipokine visfatin. Cardiovasc Res. 2011; 89:401–409. [PubMed: 20823276]
22. Zhang F, Zhang G, Zhang AY, Koeberl MJ, Wallander E, Li PL. Production of NAADP and its role in Ca2+ mobilization associated with lysosomes in coronary arterial myocytes. Am J Physiol Heart Circ Physiol. 2006; 291:H274–H282. [PubMed: 16473958]
23. Bright NA, Gratian MJ, Luzio JP. Endocytic delivery to lysosomes mediated by concurrent fusion and kissing events in living cells. Curr Biol. 2005; 15:360–365. [PubMed: 15723798]
24. Zhang F, Xia M, Li PL. Lysosome-dependent Ca(2+) release response to Fas activation in coronary arterial myocytes through NAADP: evidence from CD38 gene knockouts. Am J Physiol Cell Physiol. 2010; 298:C1209–C1216. [PubMed: 20200208]
25. Zinchuk V, Zinchuk O, Okada T. Quantitative colocalization analysis of multicolor confocal immunofluorescence microscopy images: pushing pixels to explore biological phenomena. Acta Histochem Cytochem. 2007; 40:101–111. [PubMed: 17898874]
26. Paschal BM, Shpetner HS, Vallee RB. Purification of brain cytoplasmic dynein and characterization of its in vitro properties. Methods Enzymol. 1991; 196:181–191. [PubMed: 1827862]
27. Kumar S, Lee IH, Plamann M. Two approaches to isolate cytoplasmic dynein ATPase from Neurospora crassa. Biochimie. 2000; 82:229–236. [PubMed: 10863006]

28. Neufeld TP. TOR-dependent control of autophagy: biting the hand that feeds. Curr Opin Cell Biol. 2010; 22:157–168. [PubMed: 20006481]
29. Jung CH, Ro SH, Cao J, Otto NM, Kim DH. mTOR regulation of autophagy. FEBS Lett. 2010; 584:1287–1295. [PubMed: 20083114]
30. Zhou C, Zhong W, Zhou J, Sheng F, Fang Z, Wei Y, Chen Y, Deng X, Xia B, Lin J. Monitoring autophagic flux by an improved tandem fluorescent-tagged LC3 (mTagRFP-mWasabi-LC3) reveals that high-dose rapamycin impairs autophagic flux in cancer cells. Autophagy. 2012; 8:1215–1226. [PubMed: 22647982]
31. Paglin S, Hollister T, Delohery T, Hackett N, McMahill M, Sphicas E, Domingo D, Yahalom J. A novel response of cancer cells to radiation involves autophagy and formation of acidic vesicles. Cancer Res. 2001; 61:439–444. [PubMed: 11212227]
32. Chan LL, Shen D, Wilkinson AR, Patton W, Lai N, Chan E, Kuksin D, Lin B, Qiu J. A novel image-based cytometry method for autophagy detection in living cells. Autophagy. 2012; 8:1371–1382. [PubMed: 22895056]
33. Barrachina M, Maes T, Buesa C, Ferrer I. Lysosome-associated membrane protein 1 (LAMP-1) in Alzheimer's disease. Neuropathol Appl Neurobiol. 2006; 32:505–516. [PubMed: 16972884]
34. Libby P. Atherosclerosis: disease biology affecting the coronary vasculature. Am J Cardiol. 2006; 98:3Q–9Q.
35. De Meyer GR, Martinet W. Autophagy in the cardiovascular system. Biochim Biophys Acta. 2009; 1793:1485–1495. [PubMed: 19152812]
36. Wei YM, Li X, Xu M, Abais JM, Chen Y, Riebling CR, Boini KM, Li PL, Zhang Y. Enhancement of autophagy by simvastatin through inhibition of Rac1-mTOR signaling pathway in coronary arterial myocytes. Cell Physiol Biochem. 2013; 31:925–937. [PubMed: 23817226]
37. Lacolley P, Regnault V, Nicoletti A, Li Z, Michel JB. The vascular smooth muscle cell in arterial pathology: a cell that can take on multiple roles. Cardiovasc Res. 2012; 95:194–204. [PubMed: 22467316]
38. Jia G, Cheng G, Agrawal DK. Autophagy of vascular smooth muscle cells in atherosclerotic lesions. Autophagy. 2007; 3:63–64. [PubMed: 17172800]
39. Virmani R, Kolodgie FD, Burke AP, Farb A, Schwartz SM. Lessons from sudden coronary death: a comprehensive morphological classification scheme for atherosclerotic lesions. Arterioscler Thromb Vasc Biol. 2000; 20:1262–1275. [PubMed: 10807742]
40. Clarke M, Bennett M. The emerging role of vascular smooth muscle cell apoptosis in atherosclerosis and plaque stability. Am J Nephrol. 2006; 26:531–535. [PubMed: 17159340]
41. Kimura S, Noda T, Yoshimori T. Dynein-dependent movement of autophagosomes mediates efficient encounters with lysosomes. Cell Struct Funct. 2008; 33:109–122. [PubMed: 18388399]
42. Kabeya Y, Mizushima N, Ueno T, Yamamoto A, Kirisako T, Noda T, Kominami E, Ohsumi Y, Yoshimori T. LC3, a mammalian homologue of yeast Apg8p, is localized in autophagosome membranes after processing. EMBO J. 2000; 19:5720–5728. [PubMed: 11060023]
43. Pankiv S, Clausen TH, Lamark T, Brech A, Bruun JA, Outzen H, Overvatn A, Bjorkoy G, Johansen T. p62/SQSTM1 binds directly to Atg8/LC3 to facilitate degradation of ubiquitinated protein aggregates by autophagy. J Biol Chem. 2007; 282:24131–24145. [PubMed: 17580304]
44. Lam AP, Gottardi CJ. beta-catenin signaling: a novel mediator of fibrosis and potential therapeutic target. Curr Opin Rheumatol. 2011; 23:562–567. [PubMed: 21885974]
45. Ding Z, Wang X, Schnackenberg L, Khaidakov M, Liu S, Singla S, Dai Y, Mehta JL. Regulation of autophagy and apoptosis in response to ox-LDL in vascular smooth muscle cells, and the modulatory effects of the microRNA hsa-let-7g. Int J Cardiol. 2013
46. Nowicki M, Zabirnyk O, Duerrschmidt N, Borlak J, Spanel-Borowski K. No upregulation of lectin-like oxidized low-density lipoprotein receptor-1 in serum-deprived EA.hy926 endothelial cells under oxLDL exposure, but increase in autophagy. Eur J Cell Biol. 2007; 86:605–616. [PubMed: 17643551]
47. Ding Z, Wang X, Khaidakov M, Liu S, Dai Y, Mehta JL. Degradation of heparan sulfate proteoglycans enhances oxidized-LDL-mediated autophagy and apoptosis in human endothelial cells. Biochem Biophys Res Commun. 2012; 426:106–111. [PubMed: 22910414]

48. Zhang YL, Cao YJ, Zhang X, Liu HH, Tong T, Xiao GD, Yang YP, Liu CF. The autophagy-lysosome pathway: a novel mechanism involved in the processing of oxidized LDL in human vascular endothelial cells. Biochem Biophys Res Commun. 2010; 394:377–382. [PubMed: 20223224]

49. King SM. The dynein microtubule motor. Biochim Biophys Acta. 2000; 1496:60–75. [PubMed: 10722877]

50. Lin SX, Collins CA. Regulation of the intracellular distribution of cytoplasmic dynein by serum factors and calcium. J Cell Sci. 1993; 105(Pt 2):579–588. [PubMed: 8408287]

51. Lesich KA, Kelsch CB, Ponichter KL, Dionne BJ, Dang L, Lindemann CB. The calcium response of mouse sperm flagella: role of calcium ions in the regulation of dynein activity. Biol Reprod. 2012; 86:105. [PubMed: 22262695]

52. Christensen KA, Myers JT, Swanson JA. pH-dependent regulation of lysosomal calcium in macrophages. J Cell Sci. 2002; 115:599–607. [PubMed: 11861766]

53. Pryor PR, Mullock BM, Bright NA, Gray SR, Luzio JP. The role of intraorganellar Ca(2+) in late endosome-lysosome heterotypic fusion and in the reformation of lysosomes from hybrid organelles. J Cell Biol. 2000; 149:1053–1062. [PubMed: 10831609]

54. Lloyd-Evans E, Waller-Evans H, Peterneva K, Platt FM. Endolysosomal calcium regulation and disease. Biochem Soc Trans. 2010; 38:1458–1464. [PubMed: 21118107]

55. Wu GS, Zhang YW, Wang XW, Ma ZW, Cao M, Wang QT. Effects of enamel matrix proteins loaded in chitosan thermosensitive hydrogel on bone marrow stromal cells in vitro. Shanghai Kou Qiang Yi Xue. 2009; 18:178–182. [PubMed: 19417996]

56. Xu M, Li XX, Ritter JK, Abais JM, Zhang Y, Li PL. Contribution of NADPH oxidase to membrane CD38 internalization and activation in coronary arterial myocytes. PLoS One. 2013; 8:e71212. [PubMed: 23940720]

57. Galione A. NAADP, a new intracellular messenger that mobilizes Ca2+ from acidic stores. Biochem Soc Trans. 2006; 34:922–926. [PubMed: 17052228]

58. Sasaki H, Watanabe F, Murano T, Miyashita Y, Shirai K. Vascular smooth muscle cell apoptosis induced by 7-ketocholesterol was mediated via Ca2+ and inhibited by the calcium channel blocker nifedipine. Metabolism. 2007; 56:357–362. [PubMed: 17292724]

Highlight

1. 7-ketocholesterol induces autophagy in coronary arterial myocytes.
2. Dynein mediates autophagosomes trafficking and fusion with lysosomes.
3. Lysosome-dependent NAADP-sensitive Ca^{2+} release regulates dynein ATPase activity.

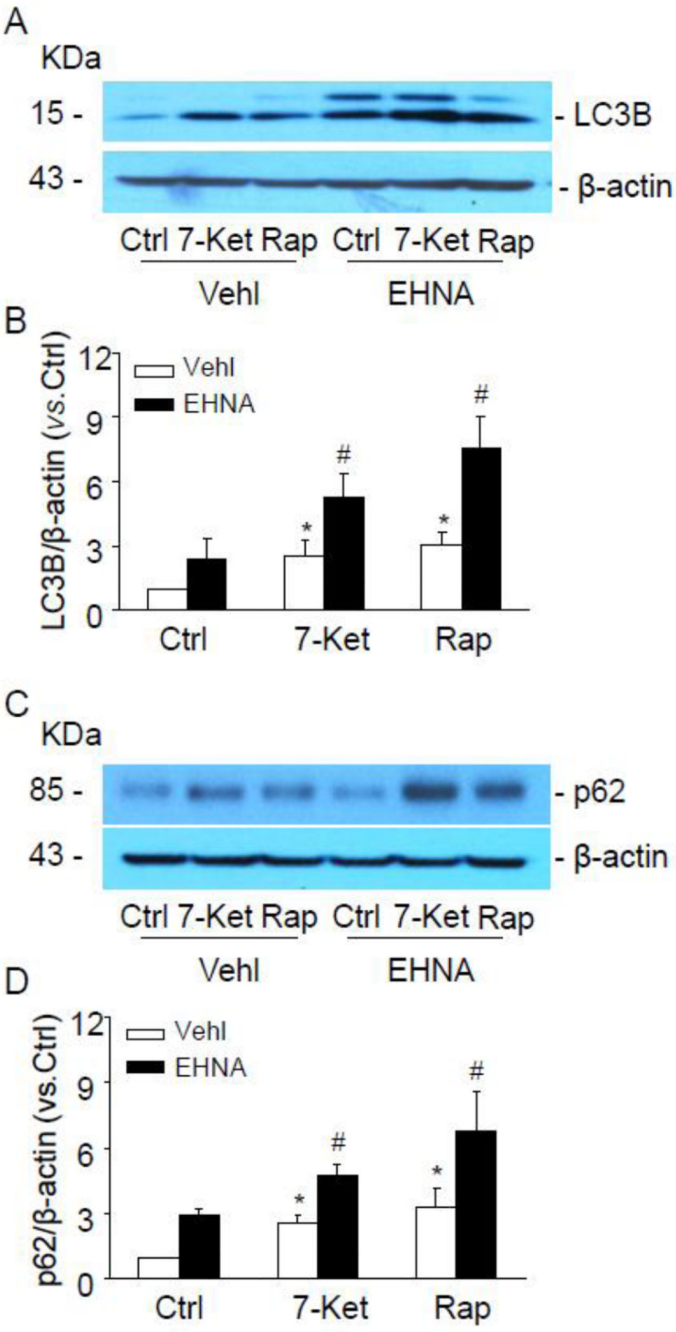

Figure 1.

The dynein inhibitor EHNA increased protein expression of LC3B and p62 upon proatherogenic stimulation. Mouse CAMs were under control conditions or stimulated with 7-ketocholesterol (7-Ket, 10 μg/mL) or rapamycin (Rap, 20 ng/mL) for 24 hours. (A, B) Representative Western blot gel document and summarized data showing the expression of LC3B in CAMs pretreated with or without EHNA (30 μM) for 30 minutes. (C, D) Representative Western blot gel document and summarized data showing the expression of p62 in CAMs pretreated with or without EHNA (n=6 for all panels). $^{*}P<0.05$ *vs.* Ctrl; $^{\#}P<0.05$ *vs.* CAMs with 7-Ket or Rap alone.

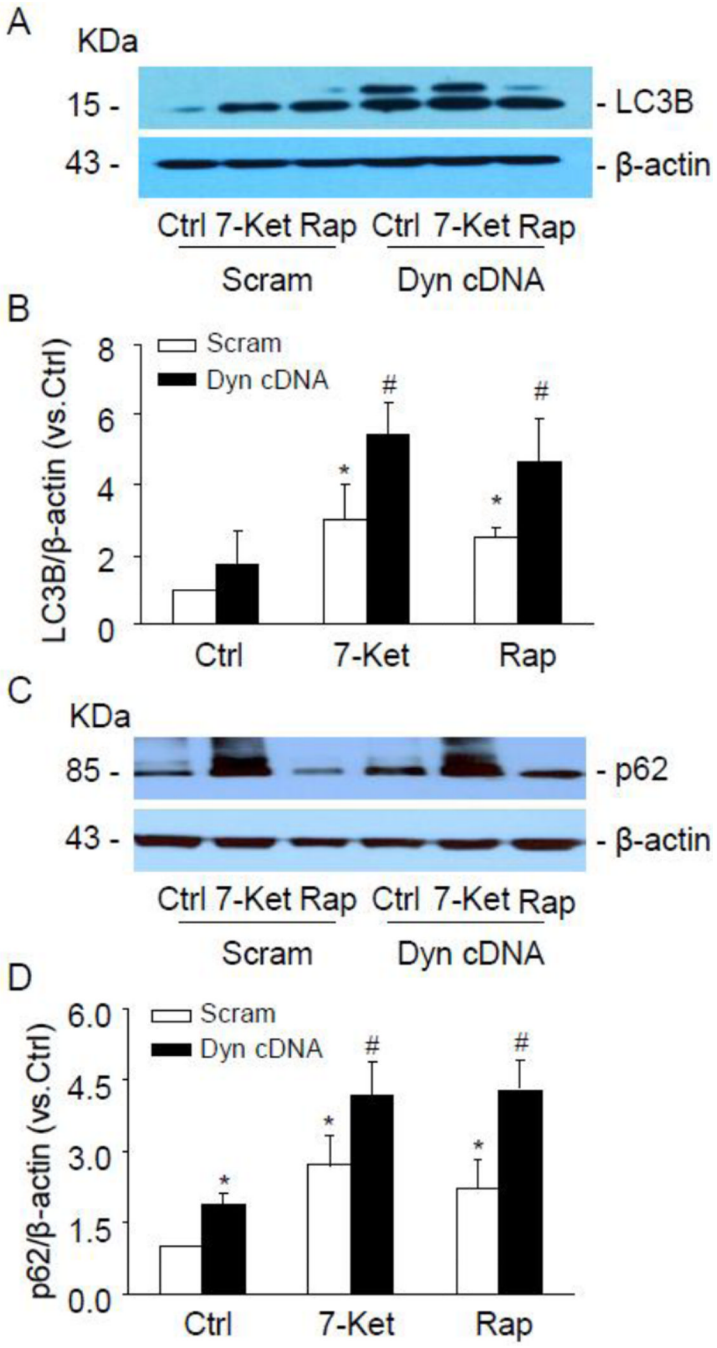

Figure 2.

Dynamitin overexpression increased the protein expression of LC3B and p62 upon proatherogenic stimulation. Mouse CAMs were left under control condition or stimulated with 7-Ket or rapamycin (Rap). (A, B) Representative Western blot gel document and summarized data showing the expression of LC3B in CAMs transfected with dynamitin cDNA. (C, D) Representative Western blot gel document and summarized data showing the expression of p62 in CAMs transfected with dynamitin cDNA (n=6 for all panels). $^{*}P<0.05$ *vs.* Ctrl; $^{\#}P<0.05$ *vs.* CAMs with 7-Ket or Rap alone.

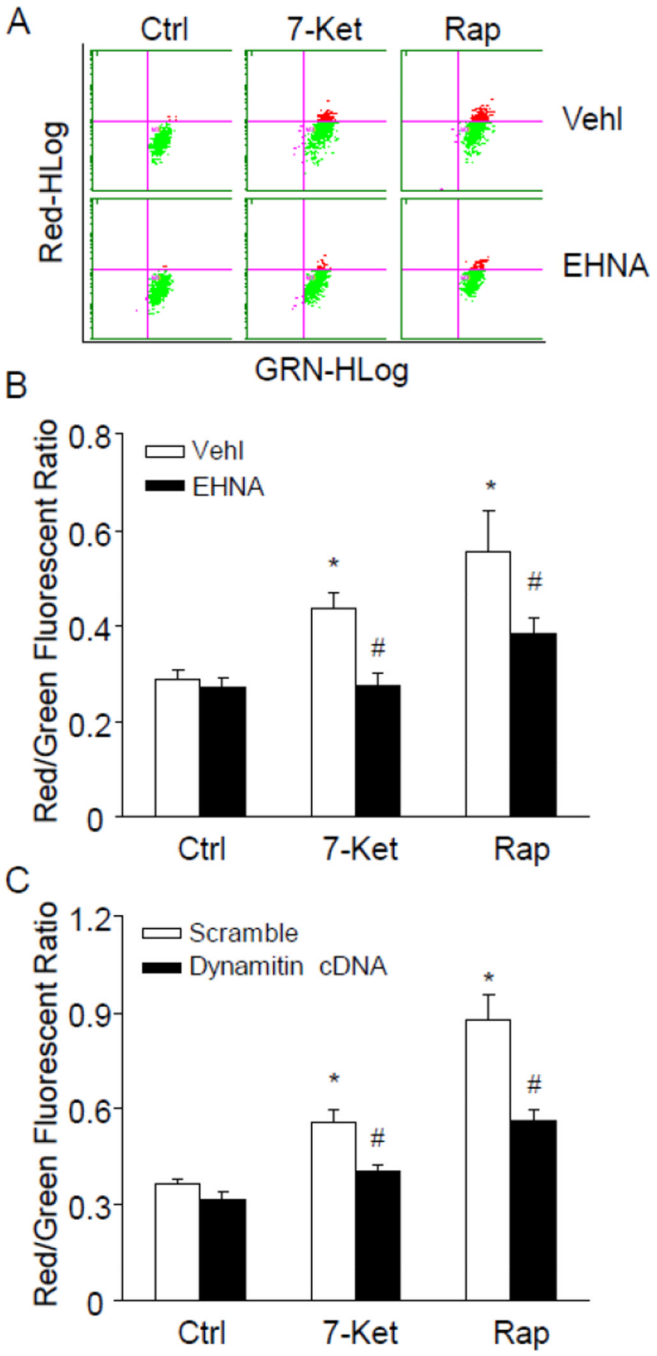

Figure 3.

Inhibition of dynein activity decreased APLs formation. Mouse CAMs were stained with acridine orange (1:5000) for 17 min. Representative dot plots of flow cytometry (A) and summarized red-to-green fluorescence ratio analysis showing APLs formation in CAMs with dynein inhibitor EHNA (B) or dynamitin overexpression (C) (n=6 for all panels). $^{*}P<0.05$ *vs.* Ctrl; $^{\#}P<0.05$ *vs.* CAMs with 7-Ket or Rap alone.

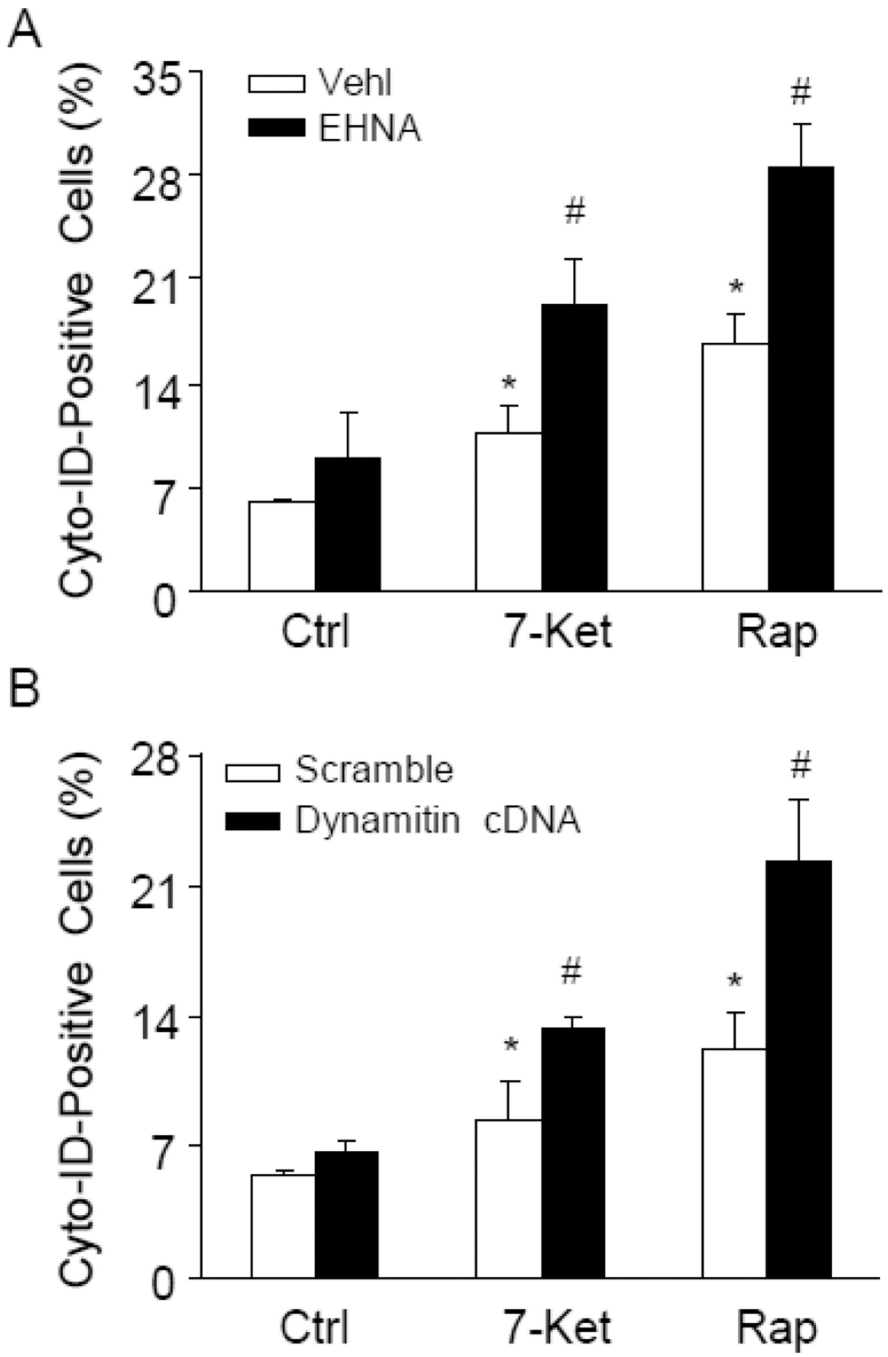

Figure 4.

Inhibition of dynein activity increased the accumulation of APs. Mouse CAMs were stained with 0.5 ml of freshly diluted CytoID fluorescent probes. Summarized percent of Cyto-ID stained cells showing the relative number of APs in CAMs with dynein inhibitor EHNA (A) or dynamitin overexpression (B) (n=6 for all panels). $^{*}P<0.05$ *vs.* Ctrl; $^{\#}P<0.05$ *vs.* CAMs with 7-Ket or Rap alone.

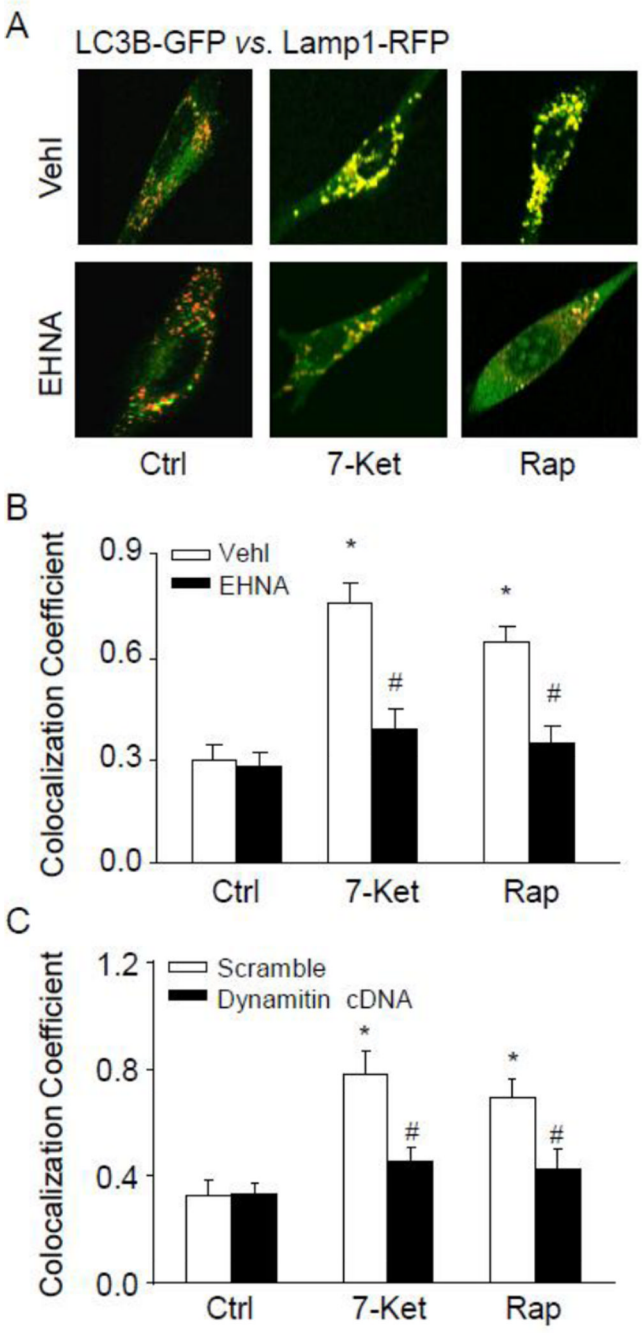

Figure 5.

Inhibition of dynein activity blocks lysosome fusion. (A) Representative confocal microscopic images showing the colocalization of LC3B-GFP with Lamp1-RFP in live CAMs. Enlarged area of interest (AOI) of merged images is presented. (B) Summarized colocalization coefficient (PCC) of LC3B and Lamp1 in CAMs with or without EHNA (n=6). (C) Summarized colocalization coefficient (PCC) of LC3B and Lamp1 in CAMs transfected with scramble or dynamitin cDNA (n=6 for all panels). $^{*}P<0.05$ *vs.* Ctrl; $^{\#}P<0.05$ *vs.* CAMs with 7-Ket or Rap alone.

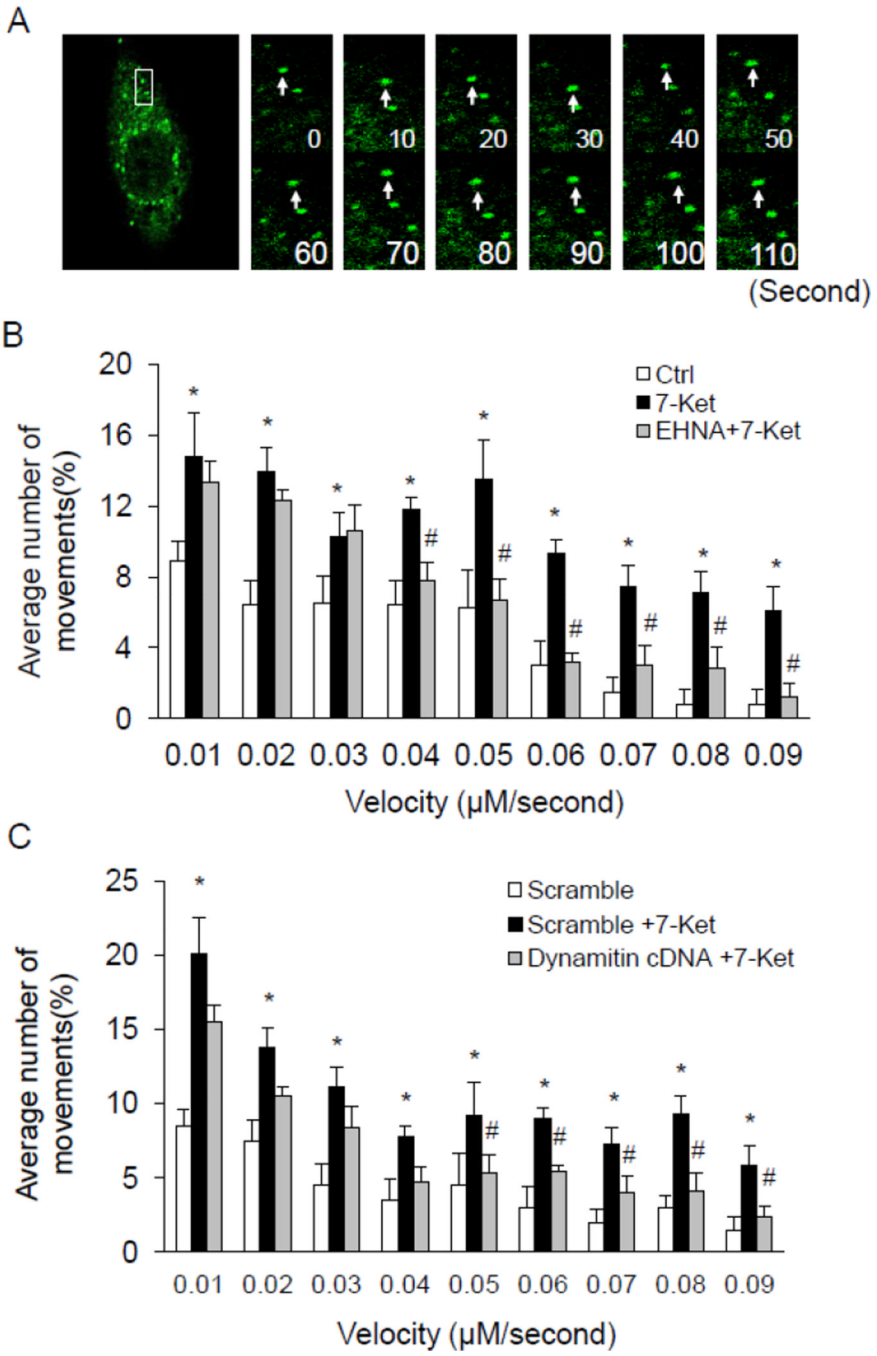

Figure 6.

Analysis to AP dynamic movements. (A) Typical fluorescent images of LC3B-GFP labeled APs were taken every 10 second in CAMs. (B, C) The summarized data show the velocity of APs in CAMs pretreated with EHNA or transfected with dynamitin cDNA (n=6 for all panels). $^{*}P<0.05$ *vs.* Ctrl; $^{\#}P<0.05$ *vs.* CAMs with 7-Ket alone.

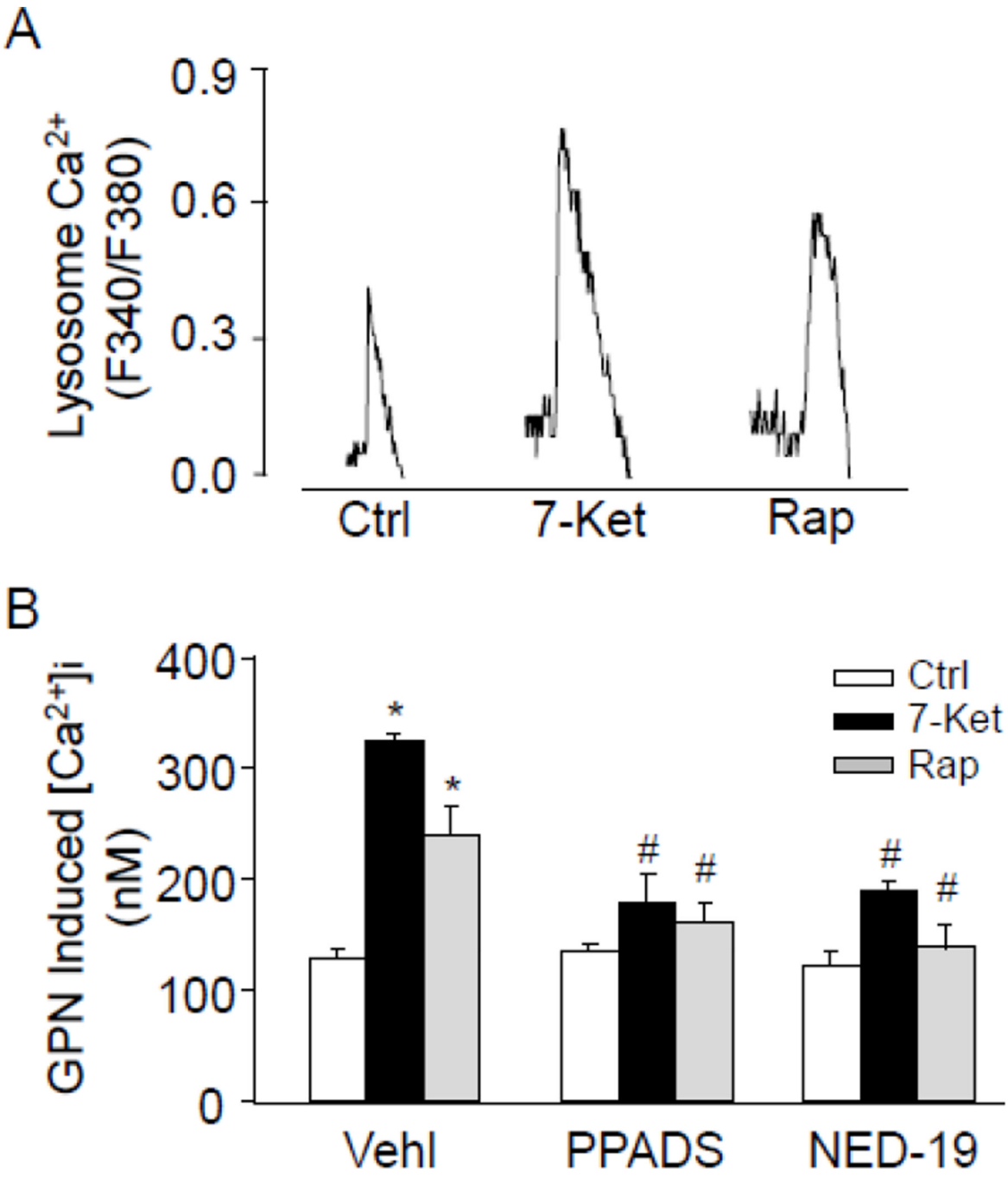

Figure 7.

Lysosome Ca^{2+} release in response to proatherogenic stimuli in living CAMs. Glycyl-l-phenylalanine-β-naphthylamide (GPN, 200 μM) was used to release Ca^{2+} from lysosomes. Representative lysosomal Ca^{2+} traces (A) and summarized data (B) showing the effects of NAADP antagonists, PPADS (50 μM) or NED-19 (10 μM) on GPN-induced lysosomal Ca^{2+} release in CAMs (n=6 for all panels). $^{*}P<0.05$ *vs.* Ctrl; $^{\#}P<0.05$ *vs.* CAMs with 7-Ket or Rap alone.

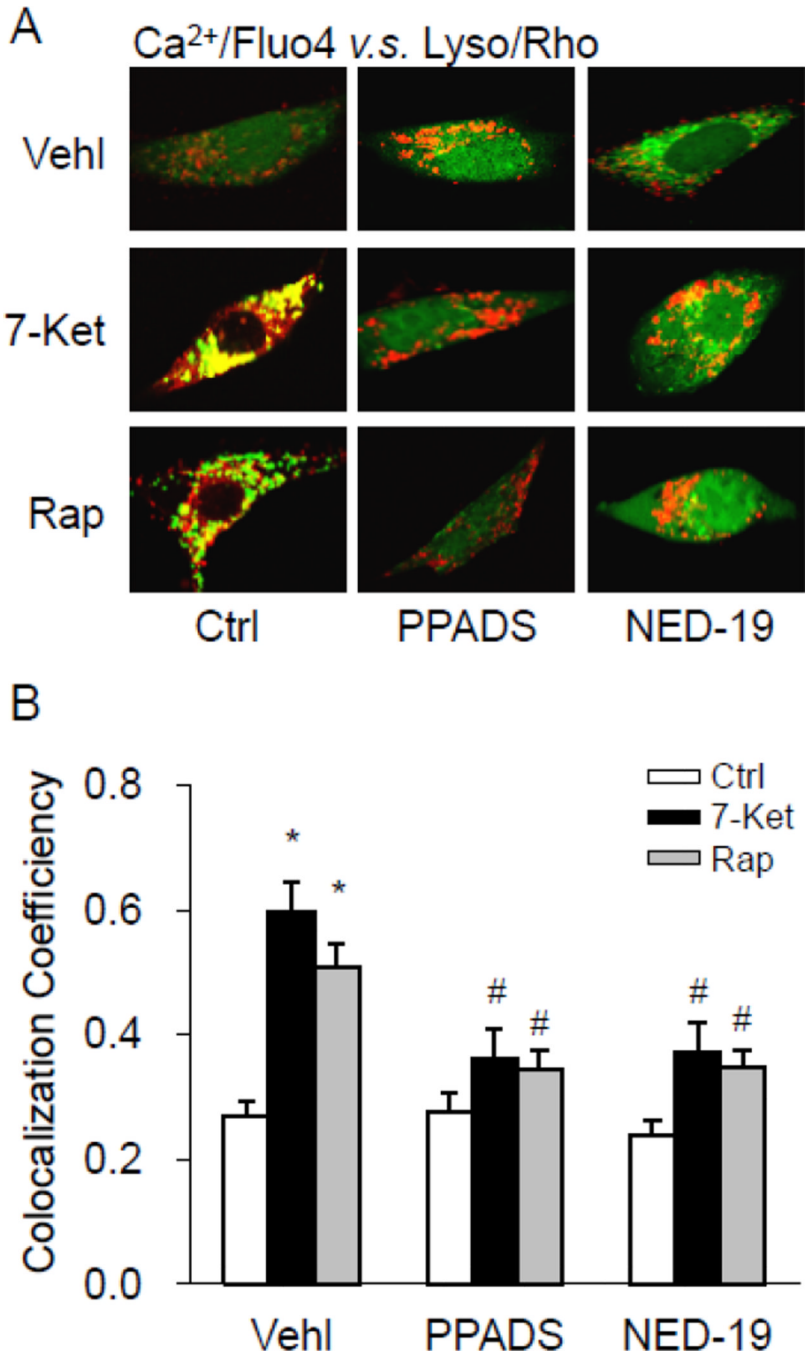

Figure 8.

Confocal microscopic detection of Ca^{2+} release from lysosomes locally in CAMs. (A) Representative confocal microscopy images showing Ca^{2+} release regions that colocalized with lysosomes as shown by yellow spots formed by green fluo-4 signals with rhodamine-red lysosomal marker (Lyso/Rho). (B) Summarized data showing the colocalization coefficiency of Ca^{2+}/fluo-4 with Lyso/Rho signals (n=6 for all panels). $^{*}P<0.05$ *vs.* Ctrl; $^{\#}P<0.05$ *vs.* CAMs with 7-Ket or Rap alone.

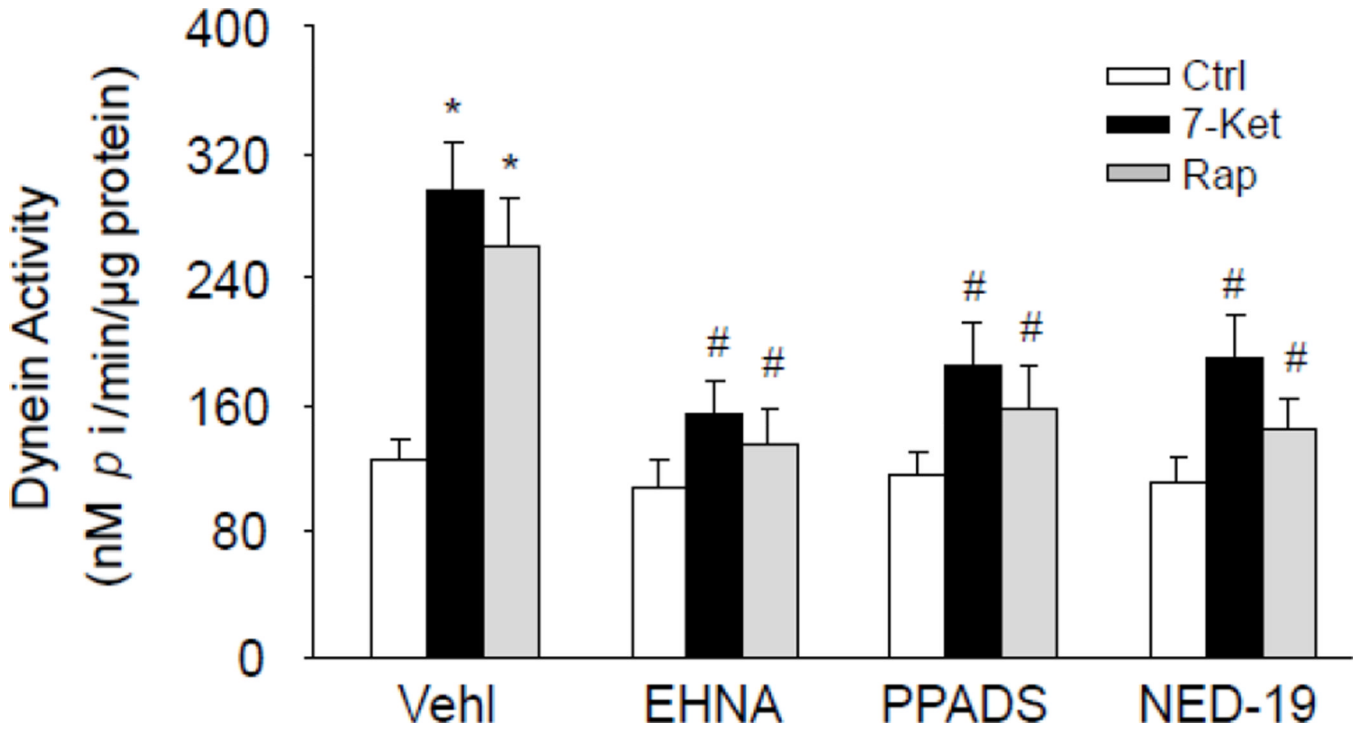

Figure 9.

NAADP-dependent lysosome Ca^{2+} controlled 7-Ket-induced dynein activity. Summarized data showing the effects of dynein inhibitor EHNA and NAADP antagonists PPADS or NED-19 on dynein ATPase activity in CAMs under control condition or with 7-Ket stimulation (n=6 for all panels). $^{*}P<0.05$ *vs.* Ctrl; $^{\#}P<0.05$ *vs.* CAMs treated with 7-Ket or Rap alone.